Electronic Supplementary Material (ESI) for Soft Matter.

Supplementary Information to

Disorder-to-order transition of long fibers contained in evaporating sessile drops

S. Sannyamath[1,2], R. Vetter[3], H. Bonart[1], M. Hartmann[1], R. Ganguly[4], S. Hardt[1]*

[1]Institute for Nano- and Microfluidics, Department of Mechanical Engineering, TU Darmstadt, Germany
[2]Department of Civil Engineering, Jadavpur University, India
[3]Computational Physics for Engineering Materials, ETH Zürich, Switzerland
[4]Department of Power Engineering, Jadavpur University, India
*Corresponding author: S. Hardt, Institute for Nano- and Microfluidics, Department of Mechanical Engineering, TU Darmstadt, Peter-Grünberg-Str. 10 64287 Darmstadt, Germany. Email: hardt@nmf.tu-darmstadt.de

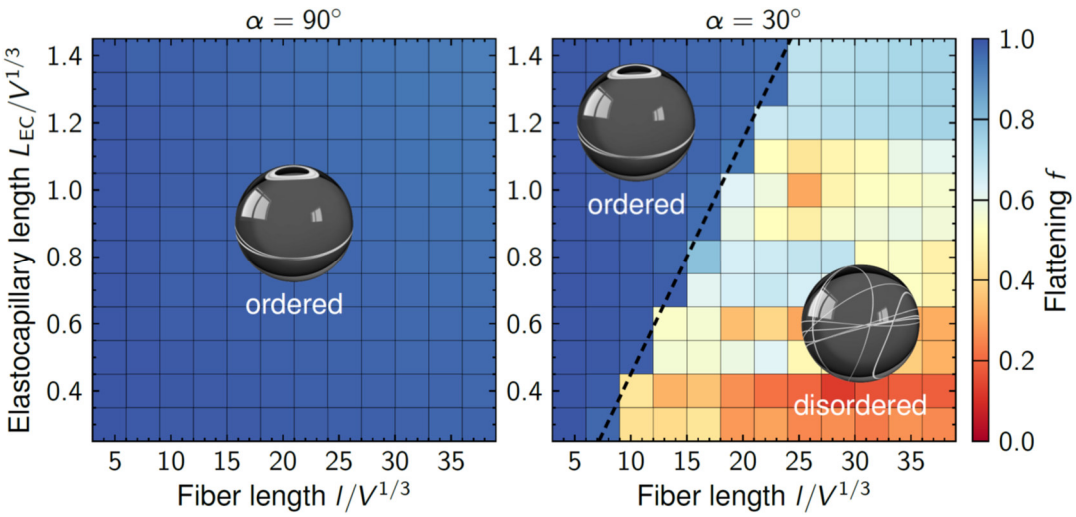

Figure S1. Morphological phase diagram analogous to Fig. 2B,C, but without considering fiber-fiber friction. See the caption of Fig. 2 for details.

As alternative measures of fiber order, we introduce two more morphological order parameters. The first one is closely related to the one originally proposed to describe order-disorder transitions of fiber packings in flexible shell confinements (Ref. 20 of the main text), but more robust to perturbations away from perfect fiber alignment. It measures the unsigned mean coiling direction of the fiber about its own principal axis of maximal moment of inertia, and is defined as follows. Denoting the fiber's centerline centroid by

$$\vec{c} = \langle \vec{x} \rangle = \frac{1}{l} \int_0^l \vec{x}(s)\, ds \tag{S1}$$

and by $\vec{v}_3$ the eigenvector with the largest eigenvalue of its 3×3 inertia tensor I about $\vec{c}$, whose components are given by

$$I_{ij} = \int_0^l \left(\|\vec{x}(s) - \vec{c}\|^2 \delta_{ij} - (\vec{x}(s) - \vec{c})_i (\vec{x}(s) - \vec{c})_j \right) ds, \;\; i,j = 1,2,3, \tag{S2}$$

$\vec{v}_3$ points along the fiber's principal axis of maximal moment of inertia. For a torus, this is always the axis of its rotational symmetry. The triple product

$$\varpi(s) = (\vec{v}_3 \times \vec{x}'(s)) \cdot (\vec{x}(s) - \vec{c}) \tag{S3}$$

is negative if the fiber turns right around the line running along $\vec{v}_3$ and passing through $\vec{c}$, and positive if it turns left around it. To measure the degree of order in the coil, the sign of this quantity is averaged over the fiber length

$$P = \langle \mathrm{sgn}(\varpi) \rangle = \frac{1}{l} \int_0^l \mathrm{sgn}(\varpi(s))\, ds. \tag{S4}$$

P vanishes if half of the fiber turns left and the other half right. For a circular coil, $P = \pm 1$, whereas for an isotropic, disordered fiber arrangement, $\vec{v}_3$ points in a random direction and $P = 0$. Since mirror-symmetric fiber configurations are considered equivalent here, we use as order parameter the coiling order magnitude $|P| \in [0,1]$. 8-shaped fibers have half of their segments turning one way and half the other, implying $|P| = 0$, whereas unidirectional ring-like coils (perfectly circular, oval, or mild perturbations of such shapes such as a saddle shape) have $|P| = 1$ (Fig. S2, left).

The phase diagram that uses $|P|$ to distinguish between ordered and disordered fiber configurations (Fig. S2) is qualitatively identical to the one using the flattening f (Fig. 2), but the disordered phase is somewhat more heterogeneous in terms of $|P|$.

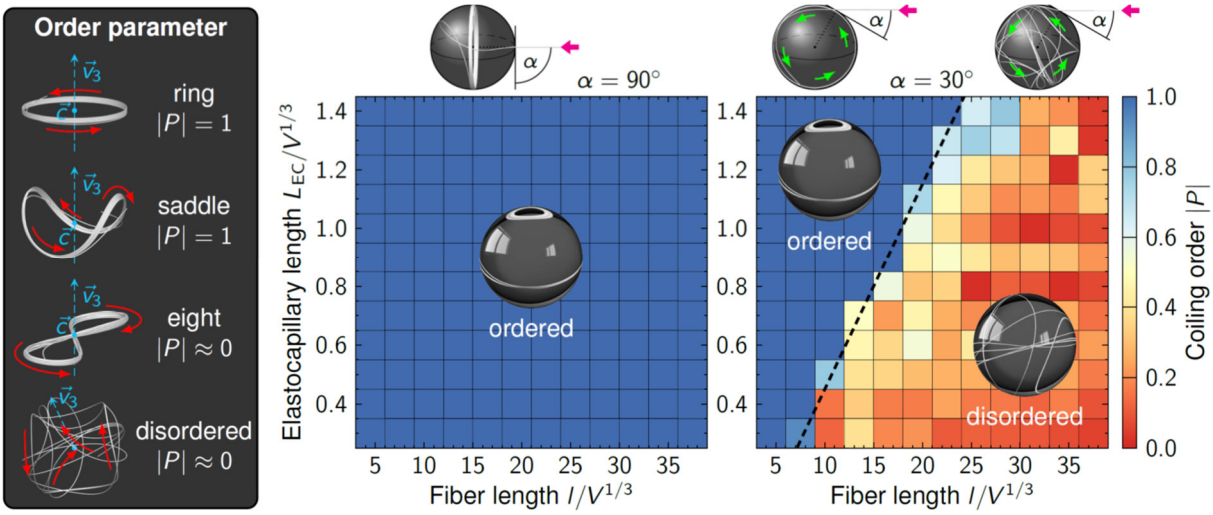

Figure S2. Order-to-disorder transition in numerical simulations analogous to Fig. 2, using the coiling order $|P|$ as the order parameter. Each colored square represents the median order parameter over 10 independent finite-element simulations.

As a third way to quantify fiber order, we borrow the notion of nematic order from liquid crystal theory and evaluate it in a local sense. Intuitively, the order in the fiber arrangement is high if adjacent fiber segments tend to be parallel, and low if they are randomly oriented or preferentially orthogonal. This is captured by the following local definition of the classical nematic order parameter S:

$$S = \langle \frac{3cos^2\theta - 1}{2} \rangle = \frac{3}{2l} \int_0^l cos^2\theta(s,a)\, ds - \frac{1}{2}, \qquad \text{(S5)}$$

where $\theta(s,a)$ is the mean angle between the fiber tangent at the arclength position s and other tangents within a local neighborhood of radius a. We use $a = 5r$ as the neighborhood size here, where r is the fiber radius, as this includes up to next-nearest neighboring fiber segments, but excludes all other segments that are further away. Distance is measured from the fiber centerline.

We observe the local nematic order S to produce a qualitatively identical phase diagram for the initial fiber configurations (Fig. S3) as f (Fig. 2) and $|P|$ (Fig. S2), notably with the same phase boundary.

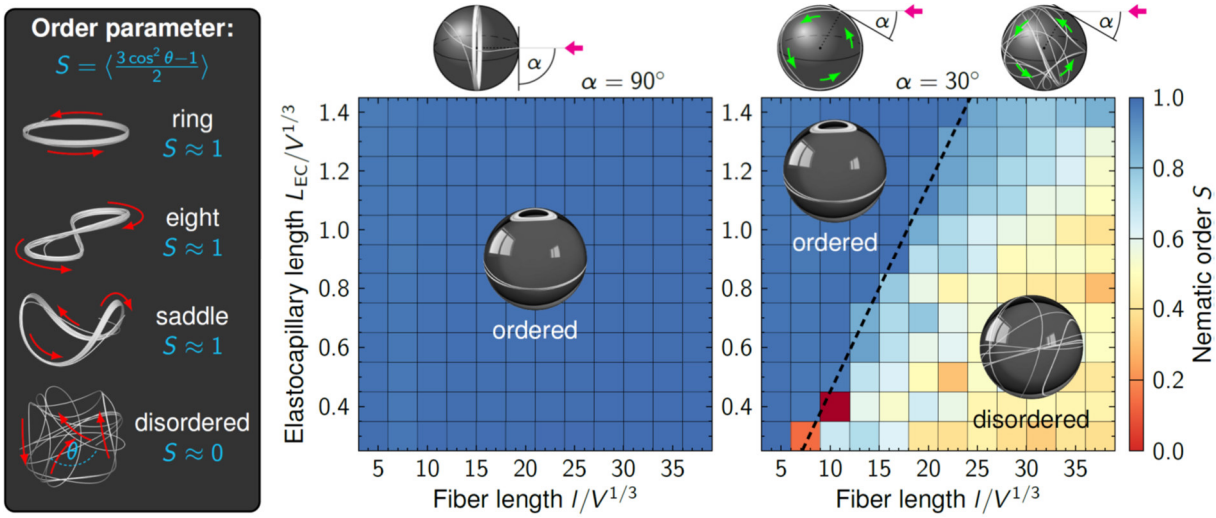

Figure S3. Order-to-disorder transition in numerical simulations analogous to Fig. 2, using the nematic order S as order parameter. The order is evaluated locally, within a neighborhood (center-to-center distance) of $5r$ within each fiber segment, where r is the fiber radius. Each colored square represents the median order parameter over 10 independent finite element simulations.

Although the order-to-disorder transition occurs for all three order parameters at the same independent system parameters, their mutual relationships are nonlinear. Figure S4 shows scatterplots for each pair of order parameters. While the flattening is never near zero for a fiber longer than $2\pi R$, the coiling order can take values arbitrarily close to zero. A coiling order of $|P| = 1$ tends to be found in 2D-like flat configurations (large f), but in particular for long fibers, can also be found in more three-dimensional fiber arrangements. On the other hand, a high degree of nematic order also tends to occur in flat fiber configurations, but is also found when the coiling order is relatively low. Finally, in rare cases with relatively short fibers, we observe negative nematic order ($S < 0$) due to nearly orthogonal fiber contacts.

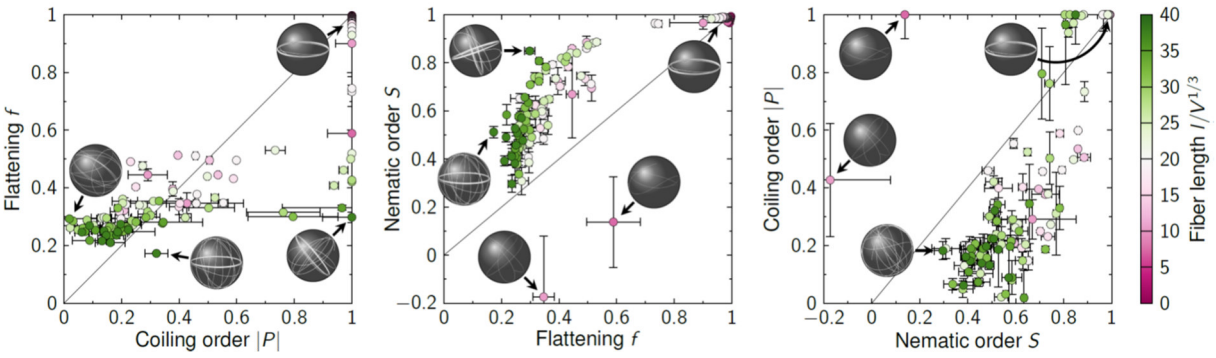

Figure S4. Pairwise comparison of different order parameters. Data points and error bars represent medians and their standard errors from 10 independent finite element simulations. Inset images show exemplary configurations to illustrate particular cases.

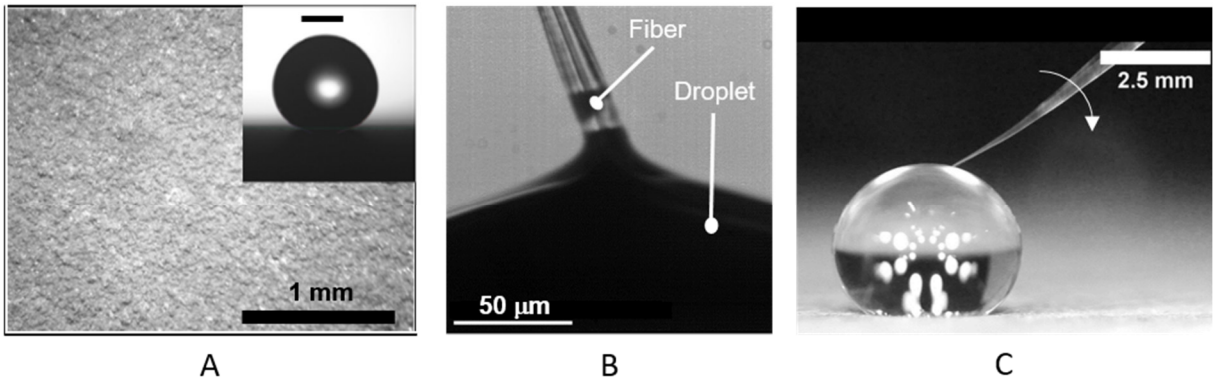

Figure S5. (A) Optical microscopy image of the superhydrophobic aluminum surface. The inset shows a water droplet on the surface. The scale bar in the inset represents 1 mm. (B) Micrograph of fiber insertion into a droplet. The liquid meniscus at the fiber indicates a contact angle ~ 0º. (C) Snapshot of a representative fiber insertion event. The overhanging part of the fiber is observed to warp around (indicated by the white arrow) the droplet immediately after contacting the liquid surface.

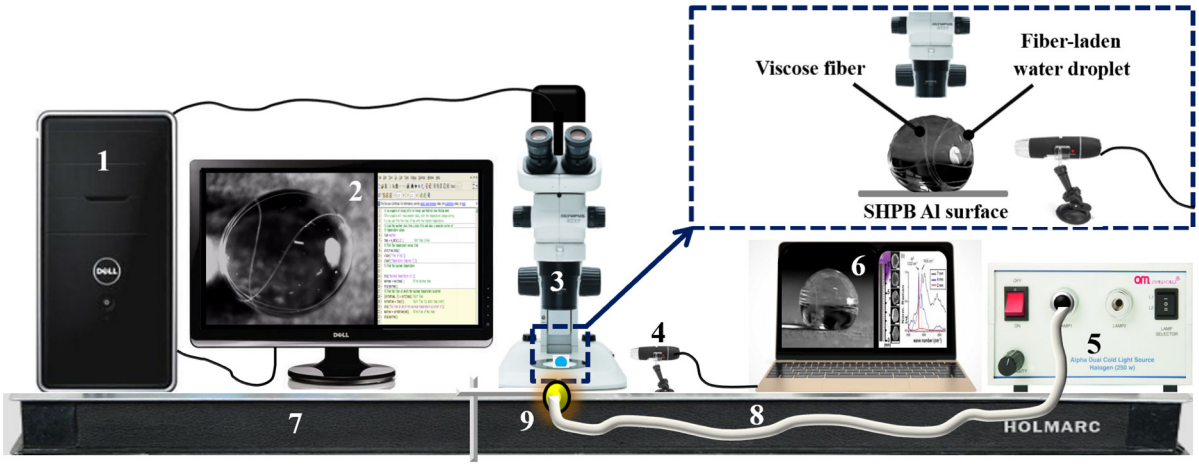

Figure S6. Schematic diagram of the experimental setup for studying the evaporation of fiber-laden droplets on superhydrophobic aluminum surfaces. Legend: 1: Desktop computer; 2: Screen-feed of the top view of a fiber-laden droplet; 3: Stereo zoom digital microscope for top view image acquisition; 4: Micro-ware 1000x USB digital microscope for side view image acquisition; 5: Cold light source for cross illumination; 6: Screen-feed of the side view of a fiber-laden droplet; 7: Optical breadboard; 8: Optical fiber for cold light; 9: Front end goose neck of the cold light source.

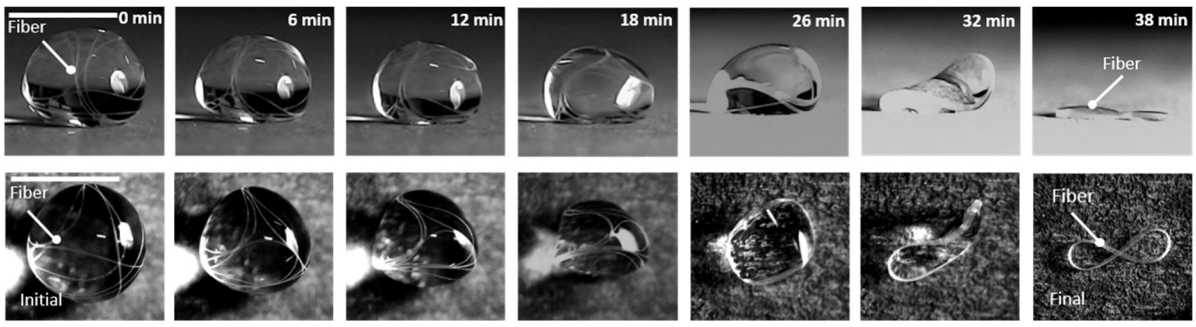

Figure S7. Time-lapse images of a 7.5 μL water droplet laden with a 50 mm long and 8 μm diameter viscose fiber, showing the morphogenesis from an initial disordered configuration to a final 8-shaped depositional pattern via a saddle-shaped transition phase. Scale bars for both side and top view images indicate 2.0 mm. The droplet evaporation time is 38 min. Sudden flipping of the coiled fiber is observed between 12 and 18 minutes.

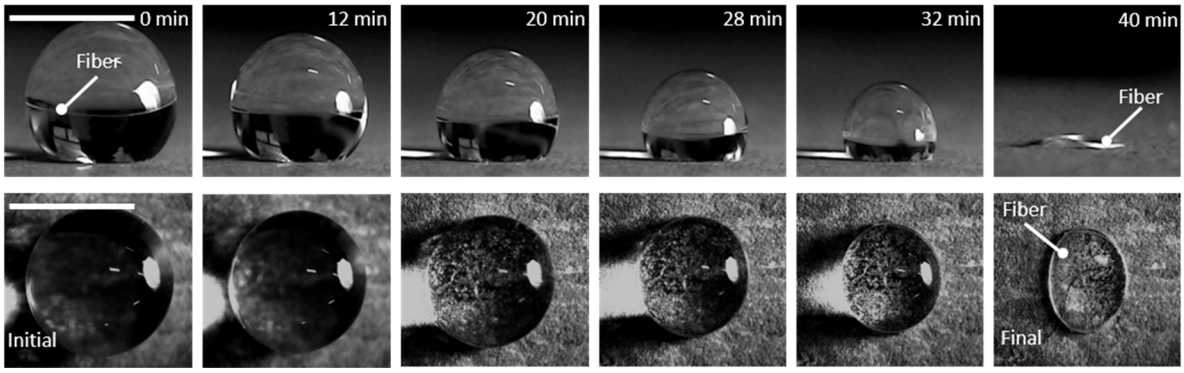

Figure S8. Time-lapse images of a 7.5 μL water droplet laden with a 10 mm long and 16 μm diameter viscose fiber, showing the morphogenesis from an initial ordered configuration to a final circle-shaped depositional pattern. The scale bars for both side and top view images indicate 2.0 mm. The droplet evaporation time is 40 min.

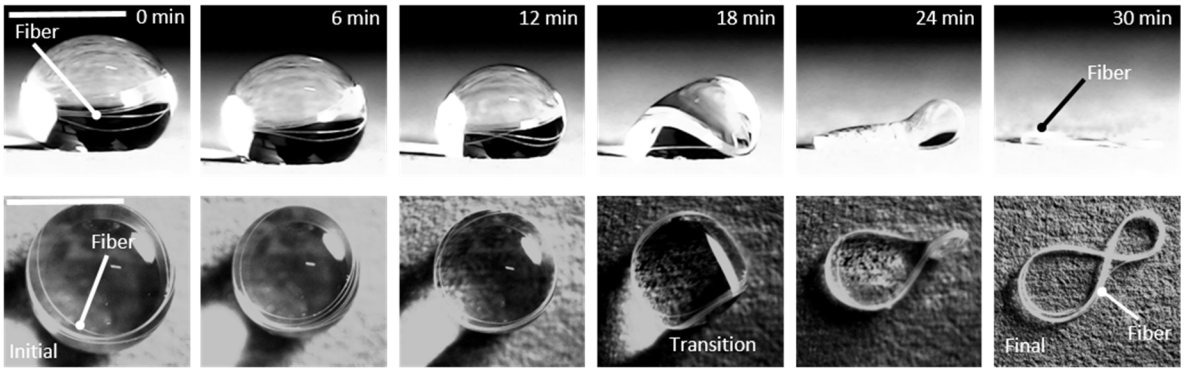

Figure S9. Time-lapse images of a 10 μL water droplet laden with a 50 mm long and 16 μm diameter viscose fiber, showing the morphogenesis from an initial ordered configuration to a final 8-shaped depositional pattern via a saddle-shaped intermediate state (occurring at ~18 minutes, marked as "transition", when the coiled fiber touches the substrate at two positions). The scale bars for both side and top view images denote 2.0 mm. The droplet evaporation time is 30 min, i.e., shorter than the evaporation time of the smaller droplets shown in Figs. S3 and S4.

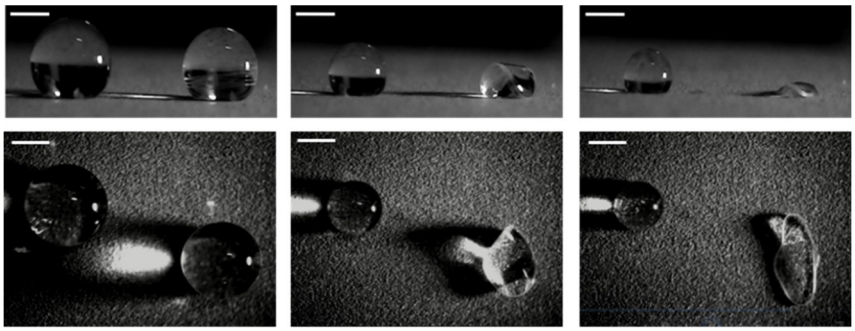

A

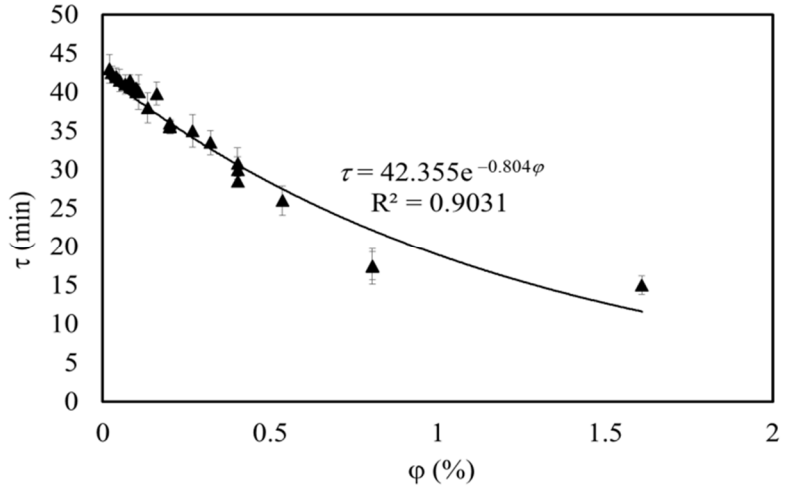

B

Figure S10. (A) Comparison of the evaporation dynamics of DI water droplets, without (left) and with a fiber (right), on a superhydrophobic aluminum surface. A representative initial droplet volume of 5.0 μL is chosen. The droplet on the right contains a 16 μm diameter and 25 mm long viscose fiber. The morphogenesis of the fiber shows a transition from an initial ordered to a final elliptical depositional pattern via an intermediate saddle morphology. The scale bars in the top and side views indicate 1 mm. (B) Plots describing the droplet lifetime τ as function of the initial fiber volume fraction φ (= fiber volume / initial droplet volume) for different combinations of fiber diameter (8 and 16 μm), fiber length (10, 25 and 50 mm) and initial droplet volumes (2.5, 5, 7.5 and 10 μL). The symbols represent experimental data, with error bars indicating standard deviations of droplet lifetimes for each set of five experiments. The line represents an exponential fit to the data. The results indicate that even a small fiber volume fraction of the order of 1 % or less has a substantial effect on the droplet lifetime.

Table S1: Parameters of the experiments

Experiment No.	Droplet volume V (µL)	Fiber diameter d (µm)	Fiber length l (mm)
1	2.5	8	50
2			25
3			10
4	2.5	16	50
5			25
6			10
7	5	8	50
8			25
9			10
10	5	16	50
11			25
12			10

Experiment No.	Droplet volume V (µL)	Fiber diameter d (µm)	Fiber length l (mm)
13	7.5	8	50
14			25
15			10
16	7.5	16	50
17			25
18			10
19	10	8	50
20			25
21			10
22	10	16	50
23			25
24			10